IAHR AIRH
Hosted by Spain Water and IWHR, China

27th IAHR International Symposium on Ice
Gdańsk, Poland, 9 – 13 June 2024

A peridynamic approach to simulate sea ice fracture with a focus on its time-dependent material behaviour

Yuan Zhang, Wenjun Lu, Raed Lubbad, Sveinung Løset, Andrei Tsarau and Knut Vilhelm Høyland
Norwegian University of Science and Technology, 7491 Trondheim, Norway

Abstract: Sea ice exhibits time-dependent non-linear behaviour. This is evidenced by both lab and field experiments with known phenomena such as creep and stress relaxation. This time-dependent material behaviour becomes particularly pronounced at larger temporal scales. In this study, we present a novel approach to simulate time-dependent fractures in sea ice using peridynamics (PD), a particle integral scheme. PD's inherent capability to handle crack initiation and multi-crack propagation offers a powerful alternative to mesh-based methods. We augment the linear-elastic constitutive relationship in the PD framework with a viscous relaxation term derived from Maxwell's theory. The failure is modelled using critical stretch criterion for the comparison with linear elastic results. Our developed model is applied to idealized simulations of sea ice deformation and fracture, providing insights into crack propagation dynamics. This work contributes to the advancement of understanding viscoelastic fracture in sea ice, offering an alternative methodology with the potential to address intricate crack problems inherent in larger-scale ice fracture scenarios.

Keywords: Sea Ice Fracture; Time-dependent non-linear behaviour, Peridynamic approach

1. Introduction

Sea ice exhibits non-linear elastic behavior with loading (and strain) rate dependence, as evidenced by both lab and field experiments (Cheng et al., 2017; Dempsey, 2002), showcasing phenomena such as creep and stress relaxation. Ice can fracture under a given load if given enough time. This behaviour of ice fracture is related to its viscoelastic properties. This viscoelastic fracture are significant phenomenon with applications in climatology, glaciology, planetology, engineering and material science (Schulson and Duval, 2009).

While numerous analytical and numerical methods (e.g., discrete crack approach and smeared damage approach etc.) have been employed to investigate the viscoelastic fracture properties of sea ice, many of these models, primarily developed through mesh-based approaches, face limitations in addressing complex crack problems (either crack track approaches and extra crack propagation criteria are required to descript explicit crack, or cracks are considered as the final consequence of damage accumulation).

Recognizing the constraints mentioned above, peridynamic theory (PD) emerges as a non-local computational approach for analyzing discontinuity problems (Silling, 2000). Peridynamics is developed utilizing integral equations rather than derivatives of displacement components, enabling the initiation and propagation of damage at any location within the deformed body. It has demonstrated successful application in identifying damage positions across various problem scenarios, including ice-structure interaction (Zhang et al., 2021a; Zhang et al., 2021b).

In this study, we present a novel model to simulate viscoelastic deformation and fracture in sea ice using PD. We augment the linear-elastic constitutive relationship in the PD framework with a viscous relaxation term derived from Maxwell's theory. Then both tension deformation and tensile fracture of sea ice is modelled and compared with existing experiment, providing insights into time-dependent behaviour and crack propagation dynamics.

This work contributes to the advancement of understanding viscoelastic fracture in sea ice, offering a valuable alternative methodology with the potential to address intricate crack problems inherent in larger-scale scenarios.

2. Numerical Model

2.1. Ordinary state-based peridynamics formulations (OSBPD)

In PD theory, the equation of motion for a material point is defined in Eq. **[1]** (Madenci and Oterkus, 2014). The discretization of the domain in PD involves particles that interact with their neighboring particles within a specific distance known as the horizon (H_x).

$$\rho(x)\ddot{\mathbf{u}}(x,t) = \int_{H_x} (\mathbf{t}(\mathbf{u}'-\mathbf{u},\mathbf{x}'-\mathbf{x},t) - \mathbf{t}'(\mathbf{u}'-\mathbf{u},\mathbf{x}'-\mathbf{x},t))dV' + \mathbf{b}(\mathbf{x},t) \qquad \textbf{[1]}$$

in which, $\mathbf{x}$ [m] and $\mathbf{x}'$ [m] represent the positions of two interacted particles in cartesian coordinate system. Under the influence of external forces (either displacement/velocity boundaries or body force $\mathbf{b}(\mathbf{x},t)$ [N/m^3]), the particles experience displacements $\mathbf{u}$ [m] and $\mathbf{u}'$ [m], respectively. Consequently, this deformation induces a force state term $\mathbf{t}$ (called force density), which has a unit of [N/m^6] acting on the one particle and another force state term $\mathbf{t}'$ [N/m^6] acting on the interacted particle in the horizon. In addition, $\rho(\mathbf{x})$ [kg/m^3] represents

the density of the sea ice, $\ddot{\mathbf{u}}(\mathbf{x},t)$ [m/s^2] is the acceleration of the discretized ice particle and V' denotes the volume of a single particle.

Madenci and Oterkus (2016) derived expression of force density with dilatational and distortional components (t^{dil} and t^{dis} respectively) and it is:

$$\mathbf{t} = (t^{dil} + t^{dis})\frac{\mathbf{y}'-\mathbf{y}}{|\mathbf{y}'-\mathbf{y}|} = (\frac{2\delta a_{dil} d}{|\mathbf{x}'-\mathbf{x}|}\theta + 2\delta b s^{dis})\frac{\mathbf{y}'-\mathbf{y}}{|\mathbf{y}'-\mathbf{y}|} \quad \textbf{[2]}$$

where δ refers to the radius of horizon, θ is dilatation. $a_{dil} = \frac{1}{2}K$, $b = \frac{6\mu}{\pi h \delta^4}$, and $d = \frac{2}{\pi h \delta^3}$ are PD parameters in 2D. s^{dis} is distortional stretch. In 2D,

$$s^{dis} = s - s^{dil} = \frac{|\mathbf{y}'-\mathbf{y}| - |\mathbf{x}'-\mathbf{x}|}{|\mathbf{x}'-\mathbf{x}|} - \frac{\delta\theta}{3|\mathbf{x}'-\mathbf{x}|} \quad \textbf{[3]}$$

2.2. Viscoelastic constitutive relation in OSBPD

Under the assumption of incompressibility in viscous fluid, the distortional force density and stretch are further decomposed into elastic part s^{dis_e} and viscous part s^{dis_vis}. Figure 1 shows 3 kinds of viscous model, and these models can be expressed by Prony series as

$$\alpha(t) = \alpha_0(1-\sum_{i=1}^{N_i}\lambda_i) + \sum_{i=1}^{N_i}\lambda_i\alpha_0 e^{-t/\tau_i} \quad \textbf{[4]}$$

in which $\alpha(t)$ is ice modulus (elastic modulus, shear modulus and bulk modulus), λ_i is a coefficient and $0 \le \sum_{i=1}^{N_i}\lambda_i \le 1$. When λ_i is closer to 0, the ice response is highly elastic while it approximately equals to Maxwell model when λ_i is closer to 1. α_0 is instantaneous modulus at time $t=0$. τ_i is time relaxation constant of ice. N_i represents the total number of Maxwell model in generalized Maxwell model, shown in Figure 1.

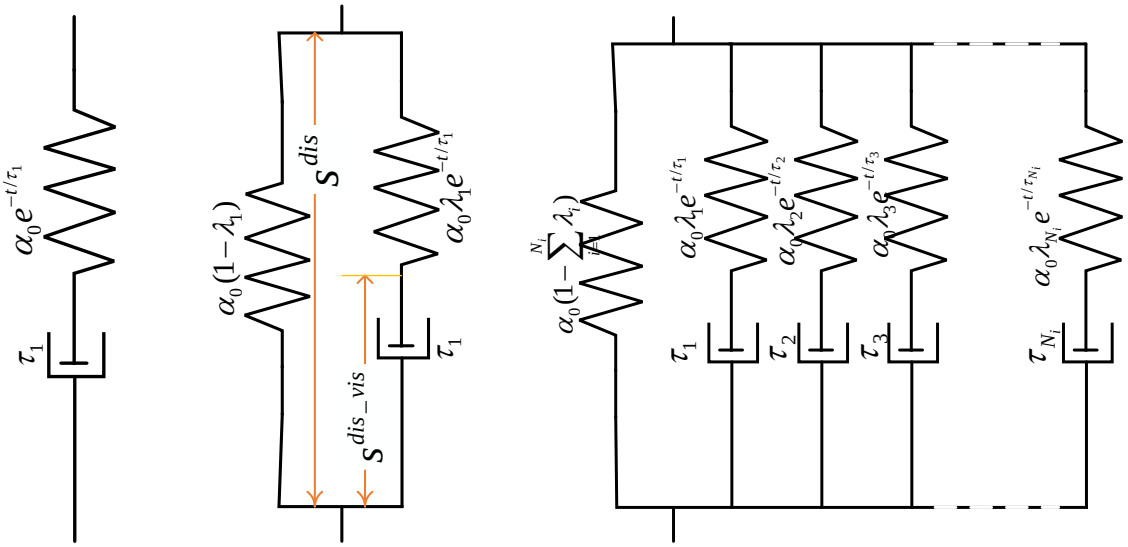

Figure 1. Viscoelastic model (left: Maxwell model; middle: standard linear solid; right: generalized Maxwell model)

With the Boltzmann principle of superposition and assumption of $s^{dis\_vis} \to 0$ when $t \to -\infty$, the force density and viscous stretch are derived (Madenci and Oterkus, 2017):

$$\mathbf{t} = (t^{dil} + t^{dis}) \frac{\mathbf{y}' - \mathbf{y}}{|\mathbf{y}' - \mathbf{y}|} = (\frac{2\delta a_{dil} d}{|\mathbf{x}' - \mathbf{x}|} \theta + (2\delta b_0 s^{dis} - \sum_{i=1}^{N_i} 2\delta b_i s^{dis\_vis}(t))) \frac{\mathbf{y}' - \mathbf{y}}{|\mathbf{y}' - \mathbf{y}|} \quad \textbf{[5]}$$

$$s^{dis\_vis}(t_{n+1}) = (1 - e^{-\Delta t/\tau_i}) s_n^{dis} + (s_{n+1}^{dis} - s_n^{dis}) + e^{-\Delta t/\tau_i} s^{dis\_vis}(t_n) - \tau_i (1 - e^{-\Delta t/\tau_i}) \frac{(s_{n+1}^{dis} - s_n^{dis})}{\Delta t} \quad \textbf{[6]}$$

2.3. Damage representation in PD

Ice failure simulation can be viewed at two levels. The first level is the particle-particle interaction elimination through a binary damage function (i.e., 0 or 1), as shown in Eq. **[7]**. The failure at this level does not necessarily entail a complete failure for a material point.

$$\Omega(t, \mathbf{x}' - \mathbf{x}) = \begin{cases} 1, \ s < s_C, & \text{unbroken or visible bond} \\ 0, \ s \geq s_C, & \text{broken or invisible bond} \end{cases} . \quad \textbf{[7]}$$

The unitless critical stretch s_C is derived from the critical energy release rate G_c [N/m]. The 2D state-based version of s_C is expressed by bulk modulus K and shear modulus μ as

$$s_C = \sqrt{\frac{G_c}{\left[\frac{6}{\pi}\mu + \frac{16}{9\pi^2}(K - 2\mu)\right]\delta}} . \quad \textbf{[8]}$$

The second level failure involves a domain damage concept in Eq. **[9]**, in which, a percentage of particle-particle interactions within the horizon of a material point is eliminated. This percentage (from 0 to 1) is termed as a damage variable and is a continuous function represents the level of 'damage', with '1' representing the complete break-off of a material point. Any other value in between 0-1 gives us the possibility to characterize the location of a macroscopic crack, e.g., with a damage variable of 0.5, it represents a crack cutting through the material point, whose 50% particle-particle connections in the horizon have been eliminated.

$$\varphi(\mathbf{x}, t) = 1 - \frac{\int_{H_x} \Omega(t, \mathbf{x}' - \mathbf{x}) dV'}{\int_{H_x} dV'} . \quad \textbf{[9]}$$

2.4. Numerical implementation and validations

The numerical implementation adopted consists of nested spatial and temporal numerical integration procedures to solve Eq. **[1]**. Following the work of Madenci and Oterkus (2014), the ice body is discretized into particles, and spatial integration is conducted within each particle's horizon to evaluate the total force acting on an ice particle at a given time. The time integration procedure tracks the positions of ice particles over time.

For dynamic solutions, the forward Euler method is utilized to compute the accelerations, velocities, and displacements at each time step. For static solutions, adaptive dynamics relaxation (ADR) techniques are utilized to achieve fast calculations under the assumption of disregarding the inertia force in viscous deformation (Kilic and Madenci, 2010).

We implemented our model in Fortran and carried out three benchmark cases to verify the constitutive model and the accuracy of the program before the sea ice study.

- The first case involves a relaxation test with two interacting particles, as described in Mitchell (2011). The force relaxation response of a single bond (interaction between

two particles) is calculated using the model described in the previous subsections and is compared with the analytical solution, matching the Figure 5 in (Mitchell, 2011).

- The second case utilizes the middle model in Figure 1 (standard linear solid) to simulate the creep response of a 1D viscoelastic bar subjected to a constant axial load and a 2D plate subjected to tension loading and unloading, respectively. The model setup and results match Fig. 4, 5, 6 presented in Galadima et al. (2023).
- The third case utilizes the generalized Maxwell model (right) in Figure 1 to simulate a viscoelastic membrane under uniaxial tension loading. This model includes a total of 15 Maxwell components. The end displacement over time agrees well with the literature, matching Fig. 8 in Madenci and Oterkus (2017).

3. Cases Study and Results

The numerical simulations for viscoelastic ice behaviour initially focus on an ice plate under tension without fracture in 2D. Subsequently, the capability to predict crack growth is demonstrated by considering the splitting of an edge-cracked rectangular ice plate in 2D.

Considering our future goal of predicting large-scale sea ice fractures rather than solely focusing on finding accurate models for small-scale sea ice damage, and based on the fact that the Maxwell model described in most literature (Dansereau et al., 2016) conforms to the time-dependent damage characteristics of large-scale sea ice, we have chosen the Maxwell model (left) in Figure 1 for these two cases. Both cases utilize ADR and have a numerical time step of $\Delta t_{ADR} = 1\,\text{s}$ and an ice viscous response time step of $\Delta t_{vis} = 1\,\text{s}$.

3.1. Creep-recovery deformation of ice

This case is inspired by the Creep-recovery test of lab-grown saline ice (Leclair et al., 1999). A rectangular plate specimen of S2 columnar saline ice was subjected to a uniform tensile stress perpendicular to the long axis of the column structure. This loading was chosen to represent the stress field occurring in the plane of natural ice covers under tension. Loading history is presented in Figure 2. Each load-hold-unload sequence was applied as a trapezoidal wave function. The stress on load-up was applied in 3 s and stress on load-release was applied in 2 s.

The length and width of the plate are specified as $L = 0.306\,\text{m}$ and $W = 0.153\,\text{m}$, respectively, with thickness, $h = 0.051\,\text{m}$. Representative model and boundary conditions are depicted in Figure. 3. Ice properties are: elastic modulus $E(t) = E_0(1-\lambda_1) + \lambda_1 E_0 e^{-t/\tau_i}$ (as explained in **Eq. [4]**) with $E_0 = 7400$ MPa, $\lambda_1 = 1.0$, and $\tau_1 = 900$ s is chosen according the theorical analysis and experiment study in Londono et al. (2016); Poisson's ratio $\nu = 0.3$; ice density $\rho = 900$ kg/m^3; bulk response is assumed elastic, and the shear response is viscoelastic as $K = \dfrac{E_0}{2(1-\nu)}$, $\mu(t) = \dfrac{E_0}{2(1+\nu)}(1-\lambda_1) + \lambda_1 \dfrac{E_0}{2(1+\nu)} e^{-t/\tau_i}$.

As for numerical concerns, the parameter is horizon size $\delta = 3\times\Delta x$ with particle spacing $\Delta x = 0.0102\,\text{m}$. Ice plate is generated with a uniform grid of 30×15 particles.

The elongation (displacement in tensions direction) of the ice plate is depicted in Figure 4. This result is compared with experiment data, elastic response and an analytical results of its primary creep response in Kavanagh and Jordaan (2022).

Despite some numerical oscillations, the Maxwell model with PD framework effectively captures the creep deformation trend of ice under tension. However, the most basic Maxwell model cannot perfectly match the creep characteristics of the lab-growth saline ice. Instead, it matches well with the primary creep behaviour of the theoretical analysis scheme. This suggests that the Maxwell model may not be entirely universal for simulating the temporal deformation behaviour of ice across multiple scales.

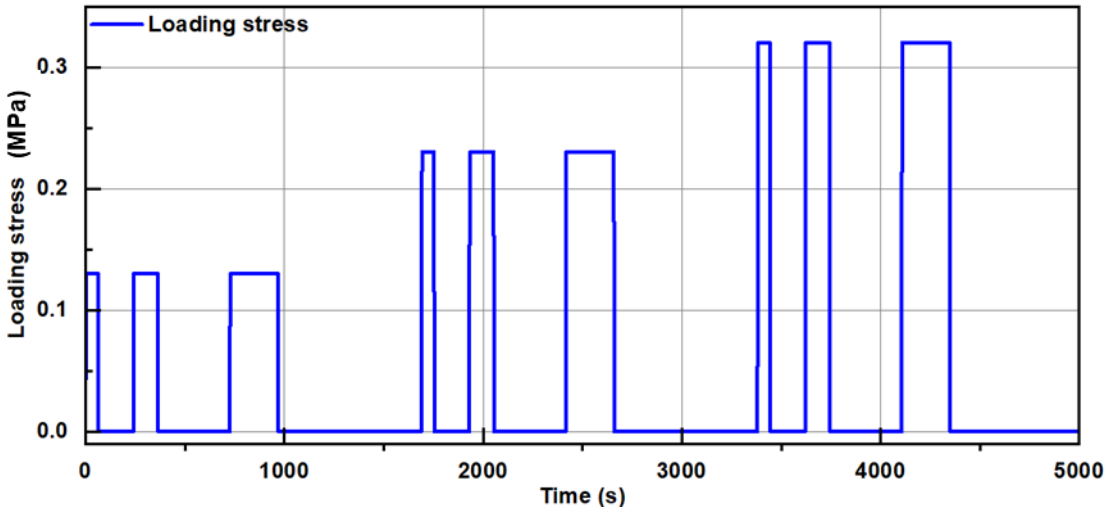

Figure 2. Loading condition (Stress vs time) for creep-recovery deformation simulation of ice

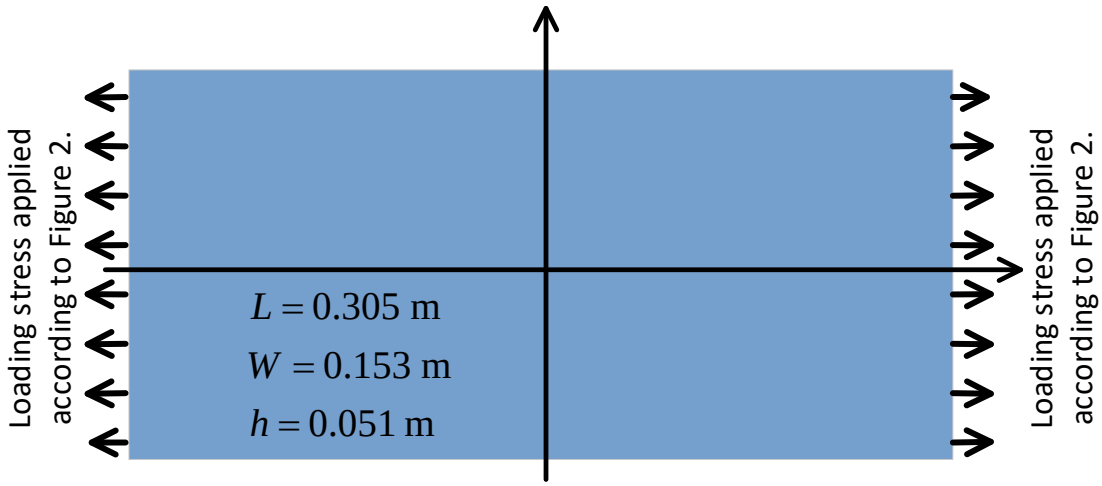

Figure 3. Representative model for creep-recovery deformation simulation of ice

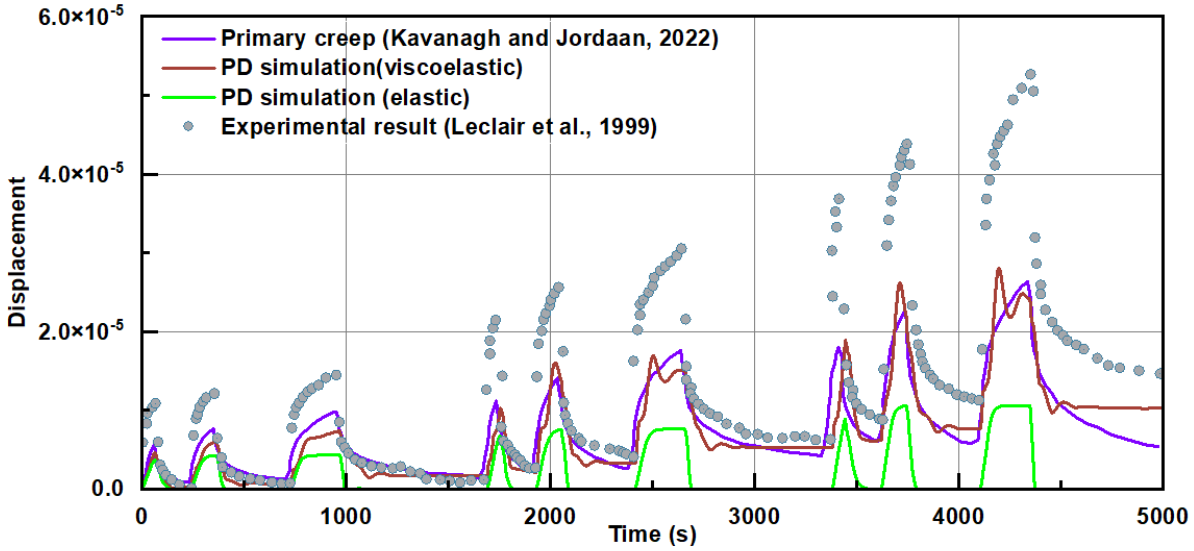

Figure 4. Result: the elongation (displacement in tensions direction) of the ice plate

3.2. Tensile fracture of viscoelastic ice

An edge cracked rectangular ice plate with length and width of $L = W = 30.0$ m, thickness of $h = 1.8$ m is modelled, as shown in Figure 5. Ice properties are: $E_0 = 5000$ MPa, $\lambda_1 = 1.0$, $\tau_1 = 900$ s, Poisson's ratio $\nu = 0.3$, ice density $\rho = 920$ kg/m^3, bulk response is assumed elastic, and the shear response is viscoelastic (calculated as the previous case).

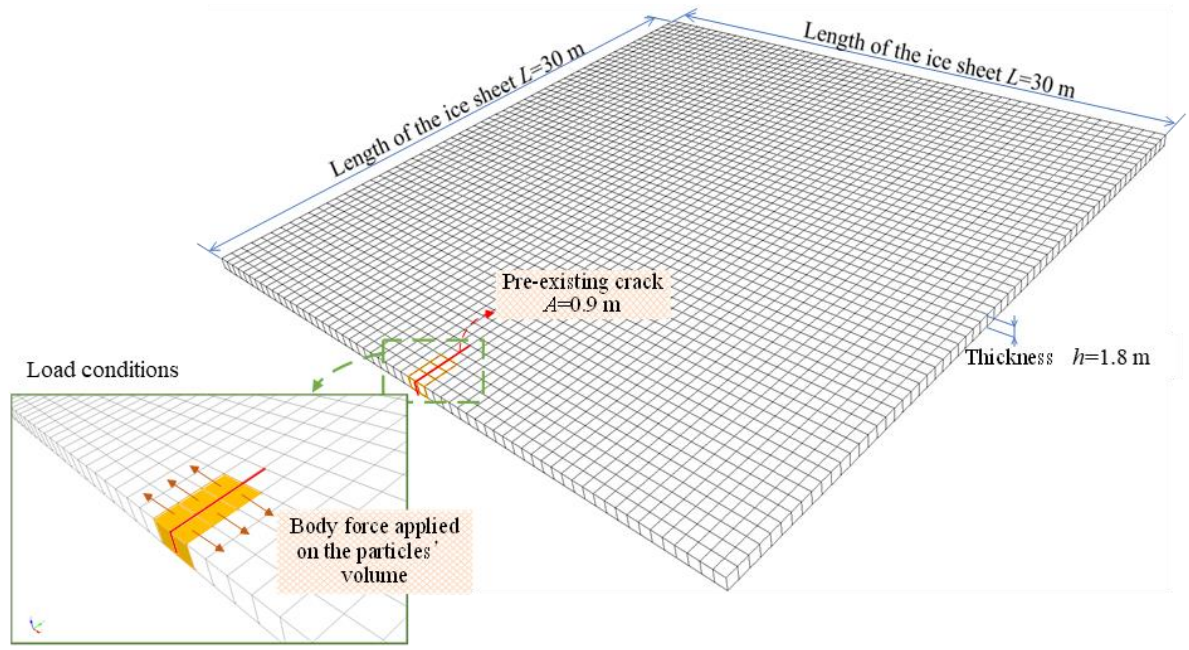

Figure 5. Model description of tensile fracture of viscoelastic ice

As for numerical concerns, the parameter is horizon size $\delta = 3 \times \Delta x$ with particle spacing $\Delta x = 0.3$ m. Ice plate is generated with a uniform grid of 100×100 particles. These parameters lead to a critical stretch of $s_C = 6.805 \times 10^{-5}$ by **Eq. [8].**

Both elastic crack growth and viscoelastic crack growth are simulated. A snap short of crack growth for both cases at the same time is illustrated in Figure 6 (e.g., $t = 1300$ s and $t = 2400$ s). We can see that there is a delay in the crack propagation for the viscoelastic

scenario. Figure 7 further illustrates this. In Figure 7, we plot the crack path length versus time for both scenarios. In viscoelastic fracture (see the orange line in Figure 7), the crack experiences creep deformation before propagating, as evident before $t = 1500$ s in Figure 7. After, the rapid increase of crack path length in viscoelastic model is captured. The crack path length versus time after 3000s if influenced by the compression failure which takes place near the top edge of the ice plate.

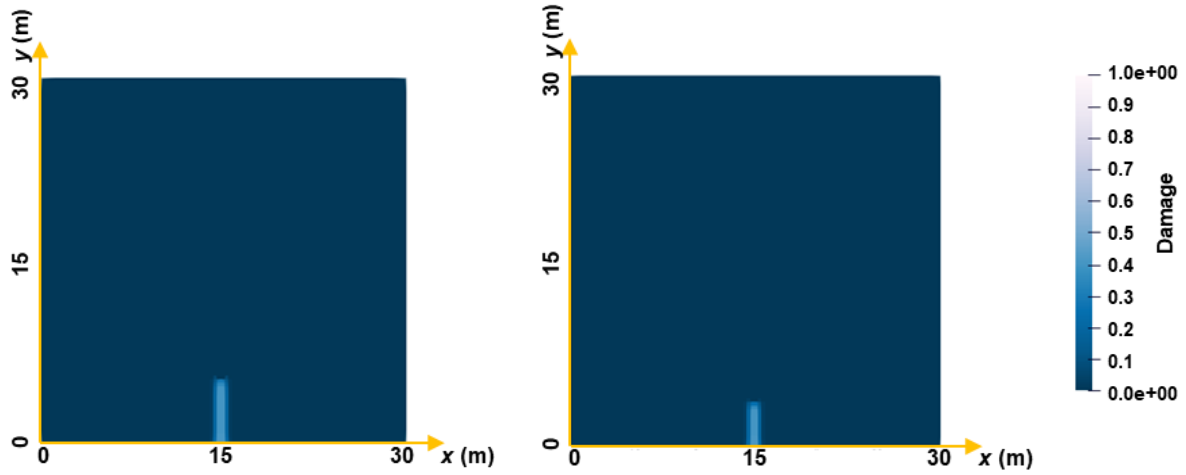

Data ①: elastic, $t = 1300$ s Data ②: viscoelastic, $t = 1300$ s

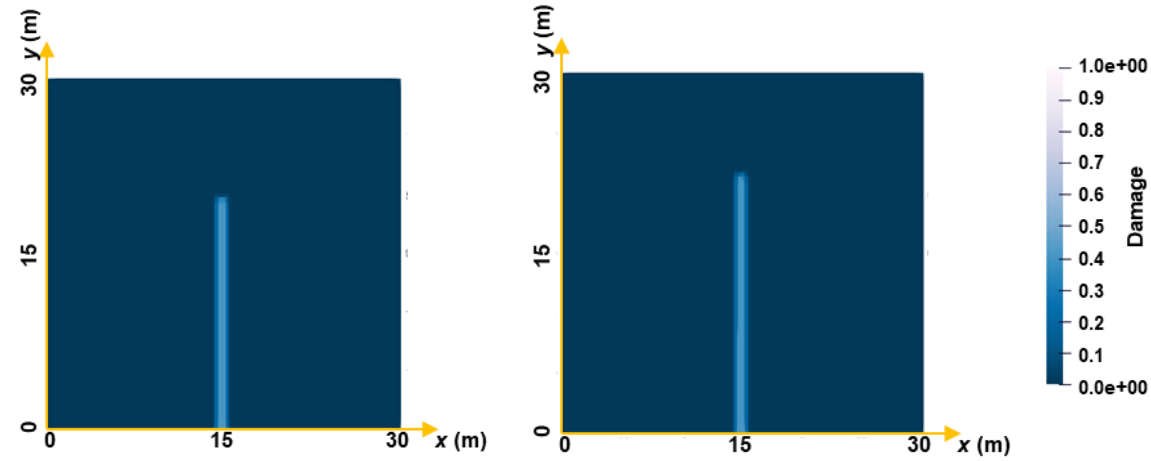

Data ③: elastic, $t = 2400$ s Data ④: viscoelastic, $t = 2400$ s

Figure 6. Crack propagation of tensile fracture of sea ice at $t = 1300$ s and $t = 2400$ s (corresponding the data point indicated in Figure 7)

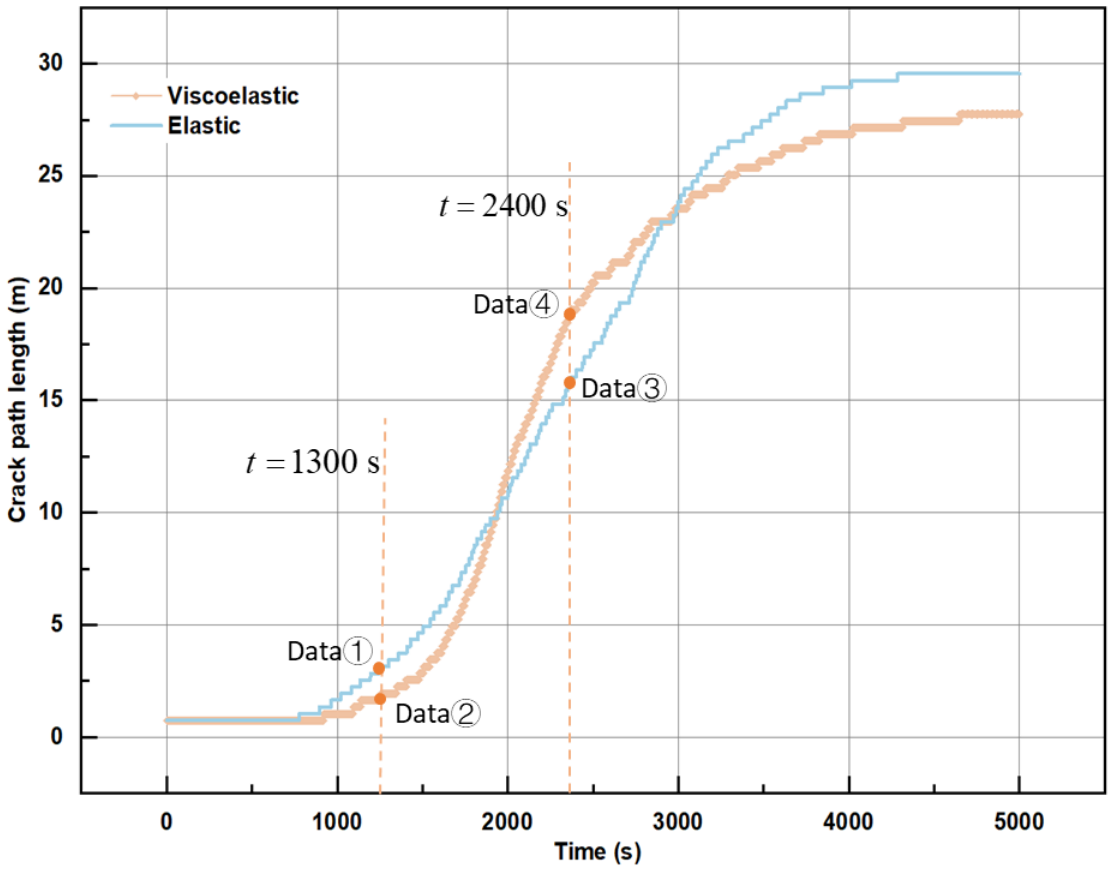

Figure 7. Time history of crack path length

4. Conclusions

The viscoelastic deformation and fracture of sea ice have been investigated using the Maxwell model within the PD framework. The creep-recovery deformation of an ice plate under tension is studied using the proposed model, revealing that while the Maxwell model, crucial for large-scale ice fracture studies, captures significant aspects of ice behavior, it may not fully simulate behavior across all scales.

The fracture of an edge-cracked rectangular ice plate under tension is preliminarily simulated using both linear elastic and viscoelastic material models. We have successfully captured some viscous-elastic fracture behaviour of sea ice, particularly the delayed fracture events and the subsequent rapid propagation in viscoelastic materials. However, further studies are necessary to comprehensively address additional properties of ice's temporal fracture behavior.

This work presents an initial study of ice's time-dependent fracture using the PD method at a small scale, laying the groundwork for our broader aim of conducting high-resolution rheological studies on ice damage at larger scales.

Acknowledgments

The authors would like to thank the Research Council of Norway for financial support through the research project “Multi-scale integration and digitalization of Arctic sea ice observations and prediction models (328960)”. We also appreciate a previous research funding from VISTA – a basic research program in collaboration between The Norwegian Academy of Science and Letters, and Equinor (former Statoil).

References

Cheng, S., Rogers, W. E., Thomson, J., Smith, M., Doble, M. J., Wadhams, P., Kohout, A. L., Lund, B., Persson, O. P. G., Collins, C. O., Ackley, S. F., Montiel, F., and Shen, H. H.: Calibrating a Viscoelastic Sea Ice Model for Wave Propagation in the Arctic Fall Marginal Ice Zone, Journal of Geophysical Research: Oceans, 122, 8770-8793, 2017.

Dansereau, V., Weiss, J., Saramito, P., and Lattes, P.: A Maxwell elasto-brittle rheology for sea ice modelling, Cryosphere, 10, 1339-1359, 2016.

Dempsey, J. P.: The Viscoelastic Fracture and Indentation of Sea Ice, Dordrecht2002, 177-186.

Galadima, Y. K., Oterkus, S., Oterkus, E., Amin, I., El-Aassar, A. H., and Shawky, H.: Modelling of viscoelastic materials using non-ordinary state-based peridynamics, Engineering with Computers, doi: 10.1007/s00366-023-01808-9, 2023. 2023.

Kavanagh, M. and Jordaan, I.: Time-dependent fracture of ice, Engineering Fracture Mechanics, 276, 2022.

Kilic, B. and Madenci, E.: An adaptive dynamic relaxation method for quasi-static simulations using the peridynamic theory, Theoretical and Applied Fracture Mechanics, 53, 194-204, 2010.

Leclair, E. S., Schapery, R. A., and Dempsey, J. P.: A broad-spectrum constitutive modeling technique applied to saline ice, International Journal of Fracture, 97, 209-226, 1999.

Londono, J. G., Berger-Vergiat, L., and Waisman, H.: A Prony-series type viscoelastic solid coupled with a continuum damage law for polar ice modeling, Mechanics of Materials, 98, 81-97, 2016.

Madenci, E. and Oterkus, E.: Peridynamic Theory and Its Applications, 2014.

Madenci, E. and Oterkus, S.: Ordinary state-based peridynamics for plastic deformation according to von Mises yield criteria with isotropic hardening, Journal of the Mechanics and Physics of Solids, 86, 192-219, 2016.

Madenci, E. and Oterkus, S.: Ordinary state-based peridynamics for thermoviscoelastic deformation, Engineering Fracture Mechanics, 175, 31-45, 2017.

Mitchell, J. A.: A non-local, ordinary-state-based viscoelasticity model for peridynamics, Sandia National Laboratories (SNL), Albuquerque, NM, and Livermore, CA 2011.

Schulson, E. M. and Duval, P.: Creep and fracture of ice, Cambridge university press, 2009.

Silling, S. A.: Reformulation of elasticity theory for discontinuities and long-range forces, Journal of the Mechanics and Physics of Solids, 48, 175-209, 2000.

Zhang, Y., Tao, L., Wang, C., Ye, L., and Guo, C.: Numerical study on dynamic icebreaking process of an icebreaker by ordinary state-based peridynamics and continuous contact detection algorithm, Ocean Engineering, 233, 2021a.

Zhang, Y., Tao, L. B., Wang, C., Ye, L. Y., and Sun, S.: Numerical study of icebreaking process with two different bow shapes based on developed particle method in parallel scheme, Applied Ocean Research, 114, 102777, 2021b.